Zero- to Ultralow-Field Nuclear Magnetic Resonance Enhanced with Dissolution Dynamic Nuclear Polarization

Román Picazo-Frutos,[1,2,*] Quentin Stern,[3,†] John W. Blanchard,[1] Olivier Cala,[3] Morgan Ceillier,[3] Samuel F. Cousin,[3] James Eills,[4] Stuart J. Elliott,[3,5] Sami Jannin,[3] and Dmitry Budker[1,2,6]

[1] *Helmholtz Institute Mainz, (Germany), GSI Helmholtzzentrum für Schwerionenforschung, 64278 Darmstadt (Germany)*
[2] *Johannes Gutenberg University, 55099 Mainz (Germany)*
[3] *Université de Lyon, CNRS, Université Claude Bernard Lyon 1, ENS de Lyon, Institut des Sciences Analytiques, UMR 5280, 69100 Villeurbanne, France*
[4] *Institute for Bioengineering of Catalonia, Barcelona Institute of Science and Technology, 08028 Barcelona, Spain*
[5] *Department of Chemistry, University of Liverpool, Liverpool L69 7ZD, United Kingdom*
[6] *Department of Physics, University of California, Berkeley, CA 94720-7300 USA*

(Dated: June 13, 2022)

Zero- to ultralow-field nuclear magnetic resonance is a modality of magnetic resonance experiment which does not require strong superconducting magnets. Contrary to conventional high-field nuclear magnetic resonance, it has the advantage of allowing high resolution detection of nuclear magnetism through metal as well as within heterogeneous media. To achieve high sensitivity, it is common to couple zero-field nuclear magnetic resonance with hyperpolarization techniques. To date, the most common technique is parahydrogen-induced polarization, which is only compatible with a small number of compounds. In this article, we establish dissolution dynamic nuclear polarization as a versatile method to enhance signals in zero-field nuclear magnetic resonance experiments on virtually all small molecules with $> 1\,\mathrm{s}$ relaxation times. We show as first examples J-spectra of hyperpolarized [^{13}C]sodium formate, [1-^{13}C]glycine and [2-^{13}C]sodium acetate. We find signal enhancements of up to 11000 compared with thermal prepolarization in a $2\,\mathrm{T}$ permanent magnet. To increase the signal in future experiments, we investigate the relaxation effects of the TEMPOL radicals used for the hyperpolarization process at zero- and ultralow-field.

I. INTRODUCTION

Nuclear magnetic resonance (NMR) is a well-established experimental method with applications in biology, chemical analysis, medical imaging, and fundamental research. Apart from the low intrinsic sensitivity in NMR, this technique suffers from two main drawbacks: First, the inability to observe signals through conductive material due to the low skin depth at high frequencies, with an exception of a few special cases, e.g. where the metal enclosure itself could be used as a resonator in a tuned circuit [1]. Second, the significant spectral broadening in heterogeneous materials due to absolute field inhomogeneity.

Recent years have seen the development of a new experimental method that overcomes these drawbacks by not requiring the use of strong magnets: zero- to ultralow-field NMR (ZULF NMR) [2]. Chemical shifts vanish in the absence of magnetic fields, however structural elucidation and chemical fingerprint can be obtained via the dominant spin-spin J-interaction [3]. ZULF NMR enables observation of signals through conductive material due to the $\nu^{-1/2}$ frequency dependence of the skin-depth in metal; the skin depth of common metals is in the μm range for radio frequencies (rf) but increases to mm for audio frequencies [4]. Furthermore, ZULF NMR is immune to magnetic-field inhomogeneities induced by heterogeneous materials, resulting in narrow lines in the order of tens of mHz [5].

ZULF NMR also offers the possibility of studying interactions invisible in conventional high-field NMR experiments, mainly limited to secular terms with respect to the high external magnetic field. Because of this, there has been an increasing interest in using zero-field NMR for research outside the Standard Model of physics, such as searching for exotic spin-spin interactions and dark matter [6, 7].

Despite the many advantages of ZULF NMR, its main limitation is low sensitivity: at zero field there is negligible spin magnetization, and therefore an external source of spin polarization is required. In early ZULF-NMR experiments, the sample was prepolarized in a magnetic field where spins reach thermal-equilibrium polarization, obeying the Boltzmann distribution of state populations, after which the sample was brought to zero field for detection [8, 9]. The disadvantage of this method is the low polarization levels that can be obtained, on the order of 10^{-6} at tesla-level fields.

An alternative approach is hyperpolarization: experimental techniques that yield nuclear spin polarization levels several orders of magnitude higher than thermal equilibrium resulting in enhanced NMR signals [10, 11]. Hyperpolarization has been particularly useful in combination with benchtop NMR devices in which thermal equilibrium polarization can be prohibitively low, since they operate at fields of no more than a few tesla [12].

* ropicazo@uni-mainz.de; These authors have contributed equally to this work
† quentin.stern@protonmail.com; These authors have contributed equally to this work

Importantly, the polarization is no longer governed by the detection magnetic-field strength, but rather the hyperpolarization method and details of the hyperpolarization procedure. Parahydrogen-induced polarization (PHIP) [13, 14] and spin-exchange optical pumping (SEOP) [15–18] have been used to hyperpolarize samples for zero- and moderate-field NMR experiments, but PHIP relies on specific chemical reactions with hydrogen gas, and SEOP is limited to polarizing noble gas atoms.

Dissolution dynamic nuclear polarization (dDNP) [19] is a more general technique, allowing one to polarize a broad variety of molecules to high polarization levels. Indeed, dDNP has established itself as the hyperpolarization method of choice for polarizing a wide range of small molecules [20, 21]. This is achieved by bringing the sample to cryogenic temperatures (typically $1.0 - 1.8\,\mathrm{K}$) commonly at fields in the 3.3 - 7 T range in the presence of unpaired electrons, whose polarization is near unity under these conditions. The electron polarization is transferred to the nuclear spins via microwave irradiation after which the frozen sample is dissolved using a hot solvent and transferred to an NMR spectrometer or MRI scanner for use of the hyperpolarized solution in the liquid state. This technique has the advantage of broad applicability, with polarization levels of tens of percent regularly achieved [22]. A first demonstration of dDNP coupled with ZULF-NMR detection was recently presented [23], where [1-^{13}C]pyruvic acid was hyperpolarized and detected with a portable zero-field spectrometer.

In this work we show an order of magnitude improvement in sensitivity, and demonstrate hyperpolarization and zero-field detection of multi-component sample mixtures. We demonstrate fine experimental control over the process, coupling the hyperpolarization apparatus with the ZULF spectrometer. We obtain spin polarization of the order of tens of percent and therefore sensitivity enhancements of 11000 with respect to a conventional ZULF-NMR experiment with sample prepolarization at 2 T.

We evaluate paramagnetic relaxation induced by the DNP polarizing agent as a possible reason for the obtained signal enhancement of 11000 while up to >50k could be expected theoretically. We discuss possible improvements of dDNP-ZULF NMR based on recently reported methods such as fast dissolution, transfer, and sample injection[24], as well as the use of filterable polarizing matrices to reduce paramagnetic relaxation [25].

II. METHODS AND EXPERIMENTAL SETUP

A. Samples

All chemicals were purchased from Sigma-Aldrich. For thermal prepolarization experiments, we used 5.2 M [^{13}C]sodium formate dissolved in D_2O, degassed by N_2-bubbling for 10 min to remove paramagnetic oxygen, which would contribute to nuclear spin relaxation.

For dDNP experiments, we used 50 mM of 4-Hydroxy-2,2,6,6-tetramethylpiperidine 1-oxyl (TEMPOL) as the polarizing agent [20]. We prepared two sample mixtures: the first mixture contained 1.5 M [2-^{13}C]sodium acetate and 1.5 M [^{13}C]sodium formate. We refer to this mixture as HP1. The second mixture, HP2, contained 0.76 M [1-^{13}C]sodium pyruvate, 0.80 M [^{13}C]sodium formate, and 0.85 M [1-^{13}C]glycine. Both samples were dissolved in $H_2O/D_2O/D_8$-glycerol $1:3:6$ ($v/v/v$), which ensures good dispersion of the radical upon freezing. This mixture is known as "DNP juice" [20, 26, 27].

B. dDNP hyperpolarization experiments

The experimental sequence consists of three steps: hyperpolarization by low-temperature DNP with cross polarization (CP), sample dissolution and transfer from the polarizer to the ZULF spectrometer, and liquid-state detection at zero field. The experimental sequence and setup are summarized in Fig. 1.

1. *Solid-state DNP*

A prototype dDNP polarizer "Alpha Polarizer" developed by *Bruker Biopspin*® was used to hyperpolarize the samples. 100 μl of HP1 or HP2 was first frozen by freezing individual 10 μl drops in liquid N_2. The resulting beads were transferred into a PEEK sample holder. In addition to the analytes, the sample holder was also loaded with 10 beads of 10 μl 3 M ascorbic acid dissolved in D_2O, as well as an additional 30 mM of sodium ascorbate to the dissolution heating module containing the hot solvent, in order to reduce the polarization loss due to paramagnetic relaxation [27]. The sample holder was placed in the liquid helium bath of the cryostat and the temperature was lowered to 1.2 K by pumping the cryostat to 0.65 mbar.

The electron polarization was transferred to the ^{1}H nuclear spins by microwave irradiation (μw) with a frequency centered at 192.65 GHz [28] and modulated at a rate of 500 Hz over a bandwidth of 160 MHz. The polarization was transferred from ^{1}H to ^{13}C spins every 4 min using microwave-gated CP as described in references [29–32]. The polarization of the ^{13}C spins during this process was monitored using 5° rf pulses applied every 30 s. As shown in Appendix A , the signal at zero field is proportional to the difference in polarization between the ^{1}H and ^{13}C spins $P(^1\mathrm{H}) - P(^{13}\mathrm{C})$ and so the signal is maximal if the respective polarizations have opposite signs. Therefore, once the polarization plateaued in the solid state, the microwave source was turned off and the ^{13}C polarization was inverted using an adiabatic frequency swept inversion pulse (chirp pulse) of 1 ms duration and 80 kHz bandwidth. At this point, the ^{1}H and ^{13}C spins had positive and negative polarization, respectively, which maximizes the signal at zero field.

2. Dissolution and transfer

The dissolution step was performed immediately after so as to minimize relaxation in the solid state. 5 ml of D_2O with 30 mM ascorbic acid was loaded into a heating module, pressurized to 6 bar with He gas and subsequently heated to 180°C corresponding to a pressure of 9 bar. The dissolution step consisted of a series of programmed events triggered by the operator. The pressurized hot solvent was injected onto the sample and pushed with He gas at 9 bar through a KelF capillary to the ZULF spectrometer. The capillary was inside a solenoid maintaining a field of 4 mT along the transfer, from the polarizer to the magnet used for thermal-prepolarization experiments. The flow of He gas was stopped after a transfer time $t_{trans} = 2$ s.

3. Injection and ZULF detection

We used a home-built ZULF spectrometer for signal detection which is a modified version of the setup described in reference [33]. Using a four-layer μ-metal shield (MS-1, Twinleaf LCC) and additional shimming coils, the residual field at the sample location was brought down to sub-nT levels. At the center of the detection region, a 3D-printed holder accommodated a standard NMR tube and a Helmholtz-coil pair along the sensitive axis (z-axis). The ZULF spectrometer was equipped with a solenoid coil to guide the sample from the prepolarization magnet to the Helmholtz coils during experiments without hyperpolarization. In the context of hyperpolarized experiments, the output of the dDNP polarizer was connected to the NMR tube inside the ZULF spectrometer *via* the prepolarization magnet and the guiding solenoid. A magnetic tunnel consisting of copper wire wound directly around the transfer capillary and fed with a current of 2 A provided a field of 4 mT along the transfer.

At the beginning of the dissolution sequence, the ZULF spectrometer received a trigger from the dDNP system, which immediately switched on the guiding solenoid and the Helmholtz-coil pair, both providing a 100 μT field. After the transfer, the hyperpolarized sample reached the NMR tube waiting in the detection region which has a PEEK assembly containing input and output capillaries for injection and exhaust. 4 s after receiving the trigger, the guiding solenoid was switched off. After an additional delay of 100 ms allowing the solenoid field to decay, the Helmholtz coil was switched off within 10 μs, bringing the spins non-adiabatically to zero field to generate an observable signal. As mentioned above, a flow of He gas pushed the solution from the polarizer during $t_{trans} = 2$ s. The detection was performed 4.1 s after the ZULF spectrometer received the trigger from the dDNP system, meaning that the solution was left at 100 μT during a settling time $t_{settle} = 2.1$ s. This delay allowed the pressure of the He propeller gas to equilibrate with atmospheric pressure for the sample to settle.

The signal was obtained via optical rotation of linearly polarized light off-resonant to the D2 transition of ^{87}Rb and circularly polarized with a laser pump beam tuned to the D1 transition of ^{87}Rb in a cross-beam laser configuration [34]. The laser beams cross in the center of a Rb vapor cell (500 torr N_2 buffer gas) with outer dimensions of $8 \times 8 \times 10\,\mathrm{mm}^3$ and 1 mm-thickness walls (Twinleaf LCC). A photoelastic modulator (II/FS42A PEM, Acal BFi Germany GmbH) was used to modulate the signal at frequencies of 50 kHz and a lock-in amplifier (SRS 830, Standard Research Systems) demodulated the signal back to audio frequencies. The demodulated signal was then acquired with an acquisition card (NI-9239, National Instruments, Austin, USA) and magnetic-field pulses and digital triggers were provided by output modules (NI-9263 and NI-9401, National Instruments, Austin,USA).

In all experiments, the atomic magnetometer had a sensitivity of 40-80 $\mathrm{fT_{rms}}/\sqrt{\mathrm{Hz}}$ in the frequency range 1-300 Hz . It is worth noting that the PEEK assembly of the sample allows the user to keep the guiding solenoid and prepolarizing magnet used in the thermal experiment, which improves the duty cycle and polarization maintenance, respectively.

4. Analyte-concentration measurement

After the measurement of ZULF spectra of hyperpolarized samples, the concentration of formate ions was measured by recording the ^{1}H NMR signal at 1.88 T on a Bruker® Fourier 80 benchtop spectrometer.

C. Thermal-polarization experiment

In order to obtain a thermal-reference comparison for our hyperpolarization experiments, we pneumatically shuttled the sample within 0.5 s using a vacuum pump from the center of a 2 T prepolarizing Halbach magnet to the detection region. Similar to the dDNP experiments, once the sample reached the center of the zero-field chamber, the guiding fields were rapidly switched off and the signal was detected. The NMR tube was assembled with PEEK pieces for efficient translation along the guiding solenoid. This is shown in the insert of Fig. 1.

III. RESULTS

A. dDNP experiments

The ZULF spectra of hyperpolarized samples HP1 and HP2 are shown in Fig. 2. A thermal-reference spectrum with prepolarization at 2 T averaged over sixteen scans of a sample of 5.2 M [^{13}C]sodium formate in D_2O is shown for comparison (black curve). The thermal-reference

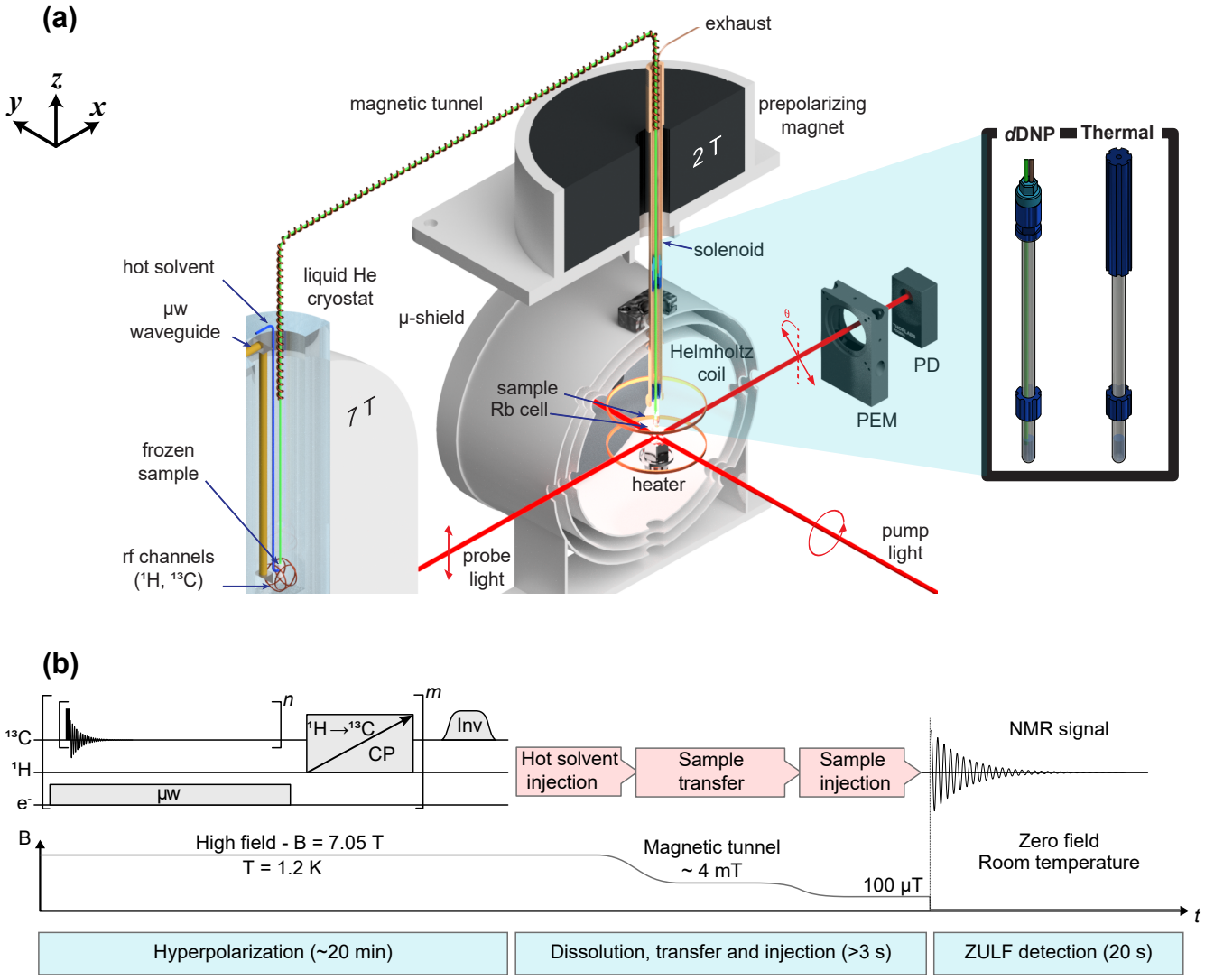

FIG. 1. **(a)** Schematic of the experimental apparatus. The sample is hyperpolarized by dDNP and is transferred to the ZULF spectrometer for detection. The spectrometer is triggered upon sample arrival and the magnetic field is suddenly switched off prior to signal acquisition. A magnetic tunnel of 4 mT maintains polarization during sample transfer. The insert shows the sample assemblies for the thermal and dDNP experiments. PEM=Photoelastic modulator, PD=photodiode. **(b)** Experimental sequence from hyperpolarization in the solid state at 1.2 K and 7.05 T to detection in the liquid state at zero magnetic field. The gray blocks "μw", "CP", and "Inv" represent μw irradiation, polarization transfer from ^{1}H to ^{13}C by cross polarization and adiabatic-inversion pulse acting on ^{13}C spins, respectively. The numbers n and m correspond to the number of ^{13}C detection blocks between each CP contact and the total number of CP contacts in the hyperpolarization scheme, respectively. Typically $n = 6$ and $m \geq 6$. Note that the 2 T magnet is omitted in the magnetic field profile of the experimental sequence.

spectrum is scaled and offset for better visualization. The noise peaks arising from the power line at 50 Hz and overtones (commonly found in ZULF NMR [33]) are grayed out, and probe-laser noise peaks are depicted with asterisks.

To understand the peaks in the ZULF spectrum it is useful to consider the Pople notation [35]. The molecules of interest can be modeled as an XA_n system, where magnetically equivalent spins A_n are equally coupled to a heteronuclear spin X. In the ZULF regime, the J-coupling interaction is dominant and causes observable transitions at integer and half-integer multiples of the J-coupling constant. In this work, we studied [^{13}C]sodium formate, [1-^{13}C] glycine, and [2-^{13}C] acetate, which correspond to XA, XA_2, and XA_3 spin systems, respectively. These systems have observable transitions at J_{XA}, $3/2\times J_{XA}$, and J_{XA} and $2\times J_{XA}$, respectively [36, 37]. The ZULF spectrum of the hyperpolarized sample HP1 features peaks at $^{1}J_{CH} = 194.7$ Hz for formate and two peaks at $^{1}J_{CH} = 127.3$ Hz and $2\times{}^{1}J_{CH}$ for acetate (see Fig. 2b).

We define the signal enhancement as the ratio between

signal integral of the hyperpolarized experiment and that of thermal reference with prepolarization at 2 T S^{DNP} and S^{th}, respectively:

$$\epsilon = \frac{S^{\mathrm{DNP}}}{S^{\mathrm{th}}}, \tag{1}$$

where it is assumed that the signals are recorded on the same sample. Because the thermal reference signal is recorded on a more concentrated sample, the enhancement ϵ is obtained by compensating for the concentration ratio between the two samples

$$\epsilon = \tilde{\epsilon}\frac{C^{\mathrm{th}}}{C^{\mathrm{DNP}}}, \tag{2}$$

where $\tilde{\epsilon}$ is the signal enhancement obtained by comparing the signal integrals of the hyperpolarized sample with that of the highly concentrated sample prepolarized at 2 T. Compared to prepolarization at 2 T, the sodium formate signal enhancement translates into a spin polarization enhancement of $\varepsilon = 5000$. Indeed, the peak shows a signal enhancement $\tilde{\varepsilon} = 44$ with a concentration of formate in the dissolved sample of HP1 determined to be 45 mM by high-field NMR, while the reference sample was at a higher concentration of 5.2 M.

In the ZULF spectrum of the hyperpolarized sample HP2, peaks can be clearly identified at ${}^1J_{\mathrm{CH}} = 194.7$ Hz for formate and there is one peak at $3/2 \times {}^2J_{\mathrm{CH}} = 8.0$ Hz for glycine (see Fig. 2c). The expected signals of pyruvate at ${}^3J_{\mathrm{CH}} = 1.4$ Hz and $2 \times {}^3J_{\mathrm{CH}} = 2.8$ Hz are not visible in the spectrum. The formate concentration in the dissolved sample was determined to be 38 mM. Compared to prepolarization at 2 T, the sodium formate peak shows a spin-polarization enhancement of $\varepsilon = 11000$ (concentration ratio of 137 and signal enhancement of $\tilde{\varepsilon} = 83$).

As we show in the Supplementary Material, the signal at zero field is proportional to the polarization difference between the ^{1}H and ^{13}C spins. Therefore, the expected enhancement is

$$\epsilon = \frac{P_I^{\mathrm{HP}} - P_S^{\mathrm{HP}}}{P_I^{\mathrm{th}} - P_S^{\mathrm{th}}}, \tag{3}$$

where P_I^{HP}, P_S^{HP}, P_I^{th} and P_S^{th} are the polarizations of the ^{1}H and ^{13}C spins in the hyperpolarization experiment and those of the thermal-reference experiment, respectively. To estimate the ^{1}H and ^{13}C polarization of the analyte that could be expected from our *d*DNP experiments, we performed a similar *d*DNP experiment on [1-^{13}C]sodium acetate injected into a Bruker Fourier 80 benchtop spectrometer operating at 1.88 T. We found ^{1}H and ^{13}C polarizations were 6 % and 20 %, respectively (see Fig. 3a). In ZULF experiments, these polarization levels would translate into an enhancement of $\varepsilon = 51000$ with respect to prepolarization at 2 T according to Eq. 3 (provided the ^{13}C spins are efficiently inverted prior to dissolution to yield $P[^{13}\mathrm{C}] = -20\,\%$). Such enhancement can be expected in the *d*DNP-ZULF experiment. However, our best-performing experiment yielded an enhancement of $\varepsilon = 11000$, less than a quarter of the expected 51000 (see Sec. IV). Figure 3b shows the signal enhancement of *d*DNP-ZULF experiments with respect to prepolarization at 2 T, calculated with Eq. 3. The result of our best-performing experiment is represented by the white bar. As both ^{1}H and ^{13}C polarization contribute to the enhancement, the value of $\varepsilon = 11000$ cannot be represented as a point on the plane but rather as a linear combination of ^{1}H and ^{13}C polarization. For example, if the ^{1}H polarization was $P[^1\mathrm{H}] = 0\,\%$, the ^{13}C polarization of the 11000-enhanced signal would be $P[^{13}\mathrm{C}] = -6.7\,\%$. The enhancement which would be achieved with the polarization levels of a state-of-the-art *d*DNP apparatus as reported in reference [38] is shown in Fig. 3 as a long-term goal for *d*DNP-ZULF NMR.

B. Paramagnetic relaxation in *d*DNP-ZULF NMR

To estimate the effect of the unpaired electrons in TEMPOL on nuclear spin relaxation [39, 40], we performed relaxometry experiments on a sample of 5.2 M [^{13}C]sodium formate diluted in D_2O using the zero-field spectrometer, for which we add TEMPOL in increasing concentration.

In each experiment, the sample was degassed by N_2-bubbling for 10 min to remove paramagnetic oxygen, which would contribute to nuclear spin relaxation. The experiments were carried out at the relevant magnetic fields used in the *d*DNP-ZULF experiments, i.e., the transfer field of 100 μT and the detection field, i.e., zero field.

We studied the relaxation rate constants for coherences $(1/T_2)$, and populations $(1/T_1)$ [36]. The results are presented in Fig. 4. The relaxation rate constants are shown on the right as a function of TEMPOL concentration, while the pulse sequence applied in each experiment is depicted on the left. The samples were prepolarized with a 2 T Halbach magnet and pneumatically shuttled into the μ-metal shield, where a Helmholtz coil provided a field of 100 μT along the sensitive axis. This field was high enough so that the spin states remain eigenstates of the Zeeman basis. The $(1/T_1)$ rate constant is determined by indirect sampling of a variable delay time τ at different fields. In Fig. 4a the sample was kept at 100 μT for a variable duration before the field was rapidly switched off prior to data acquisition.

For the measurement of $(1/T_1^{\mathrm{ZF}})$ at zero field in Fig. 4b, the field provided by the Helmholtz coil was brought down to zero within 50 ms, which was experimentally tested to ensure an adiabatic transfer to zero field. This adiabaticity ensures that the population of the Zeeman states are converted into populations of the zero-field eigenstates. After a variable time τ at zero field, a pulse of 470 μT and 100 μs duration was applied along the same axis, corresponding to a 4π- and π-pulse on proton and carbon spins, respectively. This pulse yields the max-

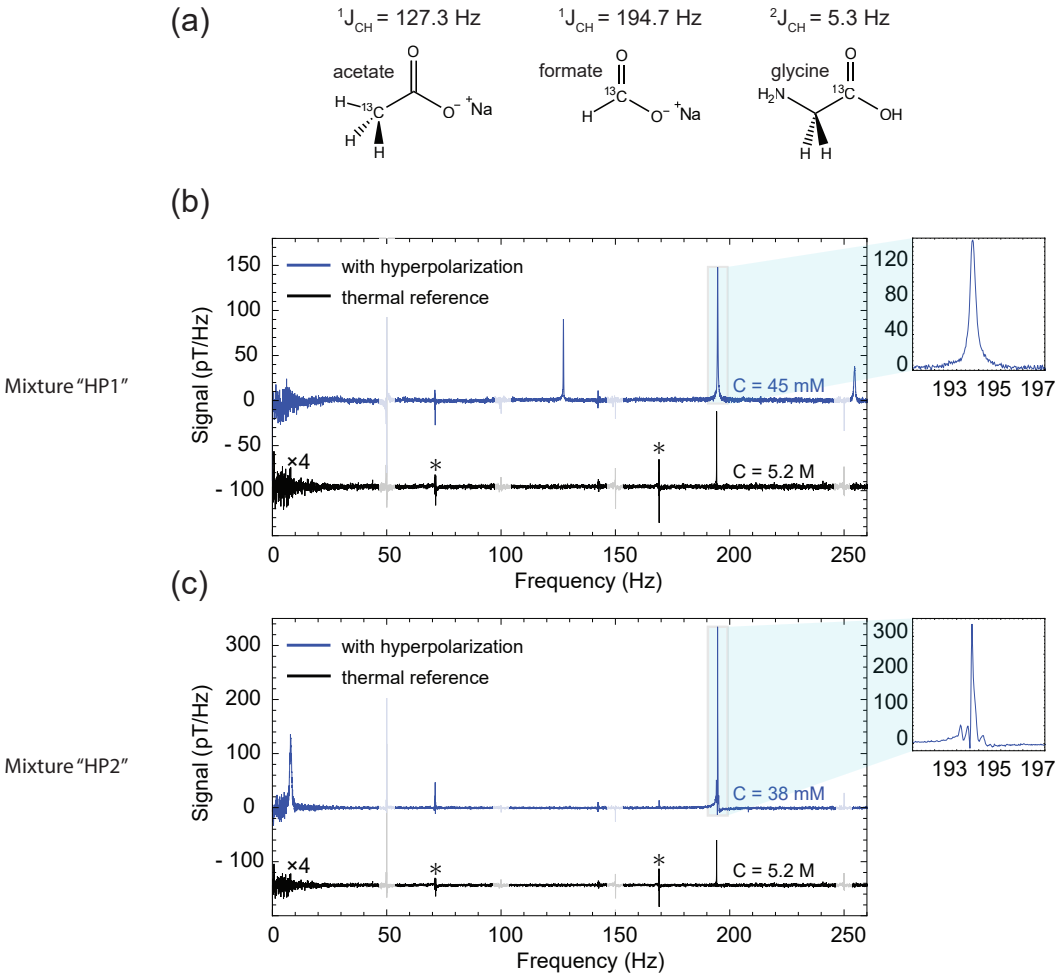

FIG. 2. ZULF spectra with *d*DNP hyperpolarization. **(a)** Molecules measured in this work. **(b)** Single-scan ZULF spectrum of the hyperpolarized sample HP1 (blue trace) compared with a reference spectrum of 5.2 M [^{13}C]sodium formate thermally prepolarized at 2T after averaging sixteen scans (black trace). The thermal-reference spectrum is rescaled and offset for better visualization. **(c)** Single-scan ZULF spectrum of the hyperpolarized sample HP2 (blue trace) compared with the same reference spectrum as in panel (a) (black trace). The noise peaks arising from the power line at 50 Hz and overtones are grayed out, and probe-laser noise peaks are depicted with asterisks. The insets show the formate peak for both mixtures with the same units.

imum signal according to Eq. A16. In Fig. 4c the NMR signals for the T_2 measurements were obtained after rapid field-drop and signal acquisition at zero field. Additionally, the stacked NMR signal is shown under the pulse sequence, broadening with increasing radical concentration.

For all measurements presented in Fig. 4, each NMR signal was fitted with a complex Lorentzian. In the case of $(1/T_1)$ measurements, the fitted values of intensity as a function of the relaxation delay τ were in turn fitted with a monoexponential function of the form $k_1 e^{-t/T_1} + k_2$, where k_1 and k_2 are constants. In the case of data taken at 100 μT, the signal should be more adequately fitted by a bi-exponential decay function [41], arising from the different relaxation rates of ^{1}H and ^{13}C spins. However, since protons contribute more greatly to the initial thermal polarization, mono-exponential fitting sufficed to fit the data with $R^2 > 0.99$. The T_2 time constant was inferred from the fitted full width at half maximum (FWHM) Γ using the relation $\Gamma = 1/(\pi T_2)$.

Assuming that the paramagnetic relaxation rates are proportional to TEMPOL concentration, we fitted the curves of relaxation rate constant as a function of TEMPOL concentration with linear functions. We found that, for each relaxation constant (T_1^{LF}, T_1^{ZF} and T_2), the TEMPOL relaxivity is $a \leq 0.3\,\mathrm{s}^{-1}\,[\mathrm{mM}]^{-1}$, where a is the fitting parameter in the inset on the right of Fig. 4. In terms of the FWHM of the signal in presence of TEMPOL, our results show that the broadening per mM of TEMPOL is $\Gamma/[\mathrm{TEMPOL}] = a/\pi \approx 100\,\mathrm{mHz/mM}$.

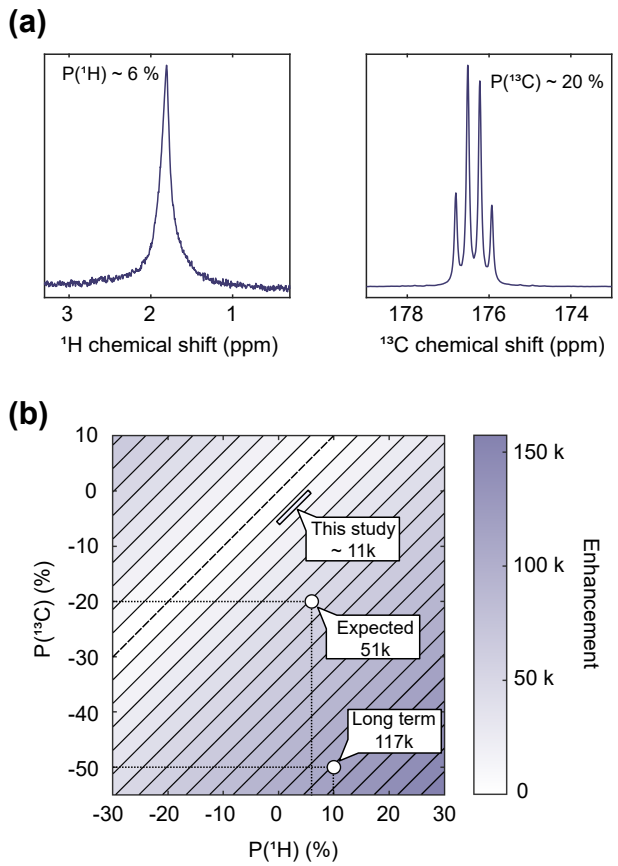

FIG. 3. **(a)** Typical results of *d*DNP experiments where a hyperpolarized sample of [1-^{13}C]sodium acetate is detected at 1.88 T for both ^{1}H and ^{13}C channels. **(b)** Map of the *d*DNP-ZULF enhancement with respect to thermal polarization at 2 T as a function of the ^{1}H and ^{13}C polarizations calculated using Eq. 3.

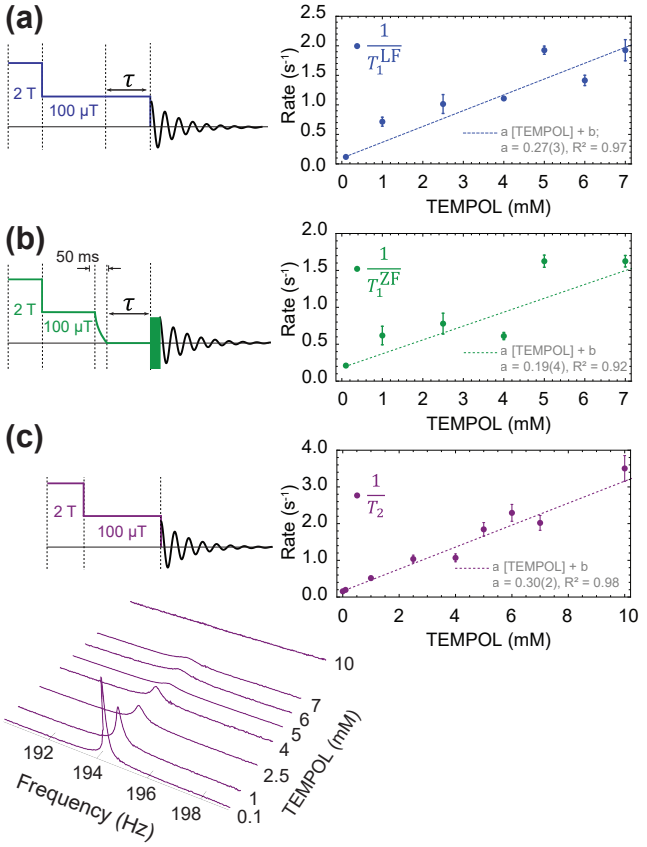

FIG. 4. Relaxation rate constants as a function of TEMPOL concentration. The sample used was 5.2 M [^{13}C]sodium formate diluted in D_2O degassed by N_2-bubbling for 10 min. For each sample, the broadening mechanism in the presence of free radicals was studied at 100 μT and zero field. The pulse sequence applied for each experiment is shown on the left, and the relaxation constant as a function of radical concentration on the right. **(a)** The sample is kept at 100 μT prior to rapid switch-off of the field and data acquisition. **(b)** The field is adiabatically switched off and a variable time is set before a π-pulse on carbon (solid block) is applied and the signal is obtained. **(c)** Linewidth of the NMR signal increases with TEMPOL concentration.

IV. DISCUSSION

The relaxometry data from Fig. 4 prove that it is possible to observe ZULF spectra of samples even in the presence of mM paramagnetic radical concentration, although at the price of significant paramagnetic broadening and therefore loss in resolution. The dissolution step of our *d*DNP experiments currently dilutes the sample by a factor of 30, bringing the TEMPOL concentration down to 1-2 mM. The concentration is further reduced by the presence of sodium ascorbate in the beads placed in the DNP sample holder and in the dissolution solvent, which acts as a scavenger for TEMPOL radicals [27]. However, the reaction between ascorbate and TEMPOL is not instantaneous. Due to the complex temperature and concentration dynamics of the dissolution step, it is not possible to know the concentration of TEMPOL precisely at the moment of injection. Considering that the TEMPOL concentration after injection is at most on the order of 1 mM, the results presented in Fig. 4 show that the broadening due to paramagnetic relaxation is expected to be within a few hundreds of mHz, acceptable for our hyperpolarized experiment. The spectra of hyperpolarized samples in Fig. 2 have linewidths of approximately 200 mHz: were this due only to TEMPOL, it would mean that 1-2 mM of radical was present at the sample at the moment of detection, consistent with our expectations. This broadening does not decrease the signal-to-noise (SNR) ratio (signal amplitude divided by the standard deviation of the nearby noise range) sufficiently to prevent us from observing hyperpolarized peaks but leads to a non-negligible signal loss during the settling time $t_{settle} = 2.1\,\mathrm{s}$. The remaining signal after 2.1 s at 100 μT for a TEMPOL concentration of 2 mM should be $\exp(-a\,[\mathrm{TEMPOL}]\,t_{settle}) \approx 0.28$ of the initial value (assuming that TEMPOL has not significantly be quenched by ascorbic acid at this point). Paramagnetic relaxation

during the transfer and settling of the solution could therefore explain why the recorded enhancement is lower than expected. This shows that increasing the speed of the transfer, shortening settling time, and suppressing paramagnetic relaxation is of paramount importance to improve the sensitivity of *d*DNP-ZULF experiments.

The SNR ratio in the ZULF spectra in Fig. 2 is only one order of magnitude higher than a single scan of the thermal reference sample, but the key difference is the hundred-fold dilution of the analytes compared with the thermal polarization experiment. Furthermore, the formate peak of Fig. 2c has SNR > 500, over an order of magnitude higher as compared with previously published work [23]. Nevertheless, the polarization levels in Fig. 3 differ from the optimum performance that could be brought by the *d*DNP apparatus by an order of magnitude. This could be due to imperfections in the magnetic tunnel leading to zero-field crossings that erode polarization, a mismatch in the synchronization of the apparatuses, or temperature and magnetic field gradients that reduce the magnetometer sensitivity. In Fig. 2 we can observe that the peak arising from glycine at 8 Hz is significantly broader than the other peaks of the hyperpolarized samples. It is well known that quadrupolar relaxation [42, 43] is significant in spin systems where nuclei with spins $> 1/2$ are involved. The broadening is possibly due to quadrupole relaxation caused by the spin-1 ^{14}N nucleus. This is important because it implies that in the zero-field detection of *d*DNP-polarized molecules such as amino acids and other nitrogen-containing molecules, the use of ^{15}N-labelled material may be necessary.

Although [1-^{13}C]pyruvate is polarized along with [1-^{13}C]glycine, it is not visible in the ZULF spectrum in Fig. 2c. We believe there are several reasons, considering that the [2-^{13}C]isotopomer was observed in previous work [23]. First, the peaks are expected at lower frequencies than those of the [2-^{13}C] isotopomer, since the ^{13}C in the first labeling position is weakly coupled to the three protons in the methyl group. As previously discussed, this XA_3 group would yield peaks at $^3J_{CH} = 1.4$ Hz and $2 \times {}^3J_{CH} = 2.8$ Hz. This poses a challenge since at very low frequencies, the magnetometer sensitivity is decreased due to $1/f$-noise. Second, pyruvate is known to have two forms in aqueous solutions, i.e., the hydrate and non-hydrate form, which show peaks at additional frequencies, which decreases the overall signal amplitude [44]. Nonetheless, these low-frequency peaks were recently observed at zero field, using PHIP as the hyperpolarization method.[45] Is it worth noting that in Fig. 2c, the formate peak shows a non-Lorentzian profile. We believe this is due to uncompensated magnetic-field gradients that hampered the shimming procedure at the sample location. This effect is also present in Fig. 2b, albeit concealed on account of a broader linewidth.

V. CONCLUSIONS AND OUTLOOK

We have established the feasibility of zero-field NMR detection of small molecules hyperpolarized via dissolution dynamic nuclear polarization. Although a limited number of molecules have been observed with parahydrogen-based hyperpolarization at zero field [46, 47], our combined experimental setup enabled us to acquire zero-field spectra of arbitrary sample mixtures thanks to the generality of *d*DNP as a hyperpolarization method, providing signal enhancements of several orders of magnitude compared with thermal prepolarization at 2T. We estimated the expected broadening due to paramagnetic relaxation of the free radicals commonly used in DNP, and found consistency with the spectra of the hyperpolarized samples.

As discussed in section IV, there is room for improvement in the SNR of the ZULF spectra by improving the sensitivity of the optically-pumped magnetometer for detection, reducing the polarization loss during sample transfer, and by increasing the concentration of hyperpolarized molecules. An appealing option to improve detection sensitivity is to employ high-sensitivity commercial optically-pumped magnetometers, which also serve to make ZULF NMR more accessible to a wider community [48].

In order to decrease the polarization losses during sample transfer, some promising methodologies can be implemented: the use of hybrid polarizing solids (HYPSOs) and hyperpolarizing polymers (HYPOPs) avoid the presence of paramagnetic radicals in the sample after dissolution which, as discussed in section III B, induces relaxation and subsequent signal loss [25, 49–51].

The use of HYPOP material as the polarizing medium will also increase the range of possible applications of *d*DNP-ZULF NMR as the use of HYPOPs is independent of the solution they host. In addition, faster dissolution and injection have been demonstrated using highly-pressurized liquids as propellers for the dissolved sample [24, 52, 53], allowing for dissolution and transfer in < 2 s. The approach taken by Kouřil et al. reduces the sample-transfer duration even further (70 ms over a 3.2 m distance demonstrated) by pneumatically shuttling the sample in the solid state [54]. These experimental advances should further improve the performance of the *d*DNP-ZULF experiment.

The implementation of this hyperpolarization technique for ZULF NMR opens up new avenues of investigations since *d*DNP can be used to polarize a broad range of molecules. For example, spectral identification of dilute material can help in monitoring chemical reactions of metabolites. As discussed in the previous section, ^{15}N-labelled material may prove useful if quadrupolar relaxation is to be avoided.

A promising application of ZULF NMR is the monitoring of catalytic chemical reactions in conditions which are relevant to industry. Burueva et al. [4] have already shown an example where ZULF NMR was combined with

PHIP hyperpolarization in order to monitor a chemical reaction with high resolution within a metal container and in presence of a heterogeneous catalyst. However, because this approach relies on PHIP hyperpolarization, it is limited to reactions where hydrogen gas is used as a reagent. Due to its low chemical specificity, *d*DNP-ZULF NMR could be used for the monitoring of a wider range of chemical reactions. ZULF is a regime where chemical reactions may be monitored with high resolution for both homogeneous and heterogeneous catalysts, due to the insensitivity of ZULF to inhomogeneities induced by the magnetic susceptibility of the sample [55, 56]. With the high sensitivity and chemical versatility offered by *d*DNP, ZULF may enable the study of the catalytic hydrogenation of unsaturated compounds or oligomerization and polymerization processes by high-resolution NMR [57].

Optimizing experimental parameters, leading to an overall enhancement of SNR, could also improve the search for dark matter with zero-field NMR, where exclusion parameters of axion and axion-like particles (ALPs) were obtained using a thermal polarization scheme [6, 7].

Our work on *d*DNP-ZULF offers competitive proton and carbon polarization and sample concentration, as well as broader applicability of target molecules, compared to techniques using parahydrogen. We expect that *d*DNP will become a standard choice of hyperpolarization for observing dilute nuclei in zero-field NMR, especially given the recently demonstrated possibility to polarize samples via *d*DNP in a remote laboratory [25].

ACKNOWLEDGEMENTS

This work was supported in part by the European Research Council (ERC) under the European Union Horizon 2020 research and innovation program (grant agreement No. 695405, ERC No. 714519 / HP4all and Marie Skłodowska-Curie No. 766402 / ZULF), by the DFG (Project ID 465084791), and by the Cluster of Excellence Precision Physics, Fundamental Interactions, and Structure of Matter (PRISMA+ EXC 2118/1) funded by the DFG within the German Excellence Strategy (Project ID 39083149). The authors gratefully acknowledge Bruker Biospin for providing the prototype *d*DNP polarizer and the F80 benchtop spectrometer for the results presented in Fig. 3, and particularly Dmitry Eshchenko, Roberto Melzi, Marc Rossire, Marco Sacher, Venita Decker, Franck Decker, and James Kempf for scientific and technical support. Catherine Jose and Christophe Pages for use of the ISA Prototype Service; and Stéphane Martinez of the UCBL mechanical workshop for machining parts of the experimental apparatus. This work was also supported by ENS-Lyon, the French CNRS, Lyon 1 University. The authors are also grateful to Lars Sperlich for helping in moving the setup from Mainz to the HMRlab in Lyon.

[1] S. Benders, M. Mohammadi, C. A. Klug, and A. Jerschow, "Nuclear magnetic resonance spectroscopy of rechargeable pouch cell batteries: beating the skin depth by excitation and detection via the casing," *Scientific reports*, vol. 10, no. 1, pp. 1–7, 2020.

[2] J. W. Blanchard and D. Budker, "Zero- to Ultralow-field NMR," *eMagRes*, vol. 5, pp. 1395–1410, 2016.

[3] J. W. Blanchard, D. Budker, and A. Trabesinger, "Lower than low: Perspectives on zero-to ultralow-field nuclear magnetic resonance," *Journal of Magnetic Resonance*, vol. 323, p. 106886, 2021.

[4] D. B. Burueva, J. Eills, J. W. Blanchard, A. Garcon, R. Picazo-Frutos, K. V. Kovtunov, I. V. Koptyug, and D. Budker, "Chemical reaction monitoring using zero-field nuclear magnetic resonance enables study of heterogeneous samples in metal containers," *Angewandte Chemie International Edition*, vol. 59, no. 39, pp. 17026–17032, 2020.

[5] J. W. Blanchard, M. P. Ledbetter, T. Theis, M. C. Butler, D. Budker, and A. Pines, "High-resolution zero-field nmr J-spectroscopy of aromatic compounds," *Journal of the American Chemical Society*, vol. 135, no. 9, pp. 3607–3612, 2013.

[6] A. Garcon, J. W. Blanchard, G. P. Centers, N. L. Figueroa, P. W. Graham, D. F. J. Kimball, S. Rajendran, A. O. Sushkov, Y. V. Stadnik, A. Wickenbrock, *et al.*, "Constraints on bosonic dark matter from ultralow-field nuclear magnetic resonance," *Science advances*, vol. 5, no. 10, p. eaax4539, 2019.

[7] T. Wu, J. W. Blanchard, G. P. Centers, N. L. Figueroa, A. Garcon, P. W. Graham, D. F. J. Kimball, S. Rajendran, Y. V. Stadnik, A. O. Sushkov, *et al.*, "Search for axionlike dark matter with a liquid-state nuclear spin comagnetometer," *Physical Review Letters*, vol. 122, no. 19, p. 191302, 2019.

[8] M. C. Tayler, T. Theis, T. F. Sjolander, J. W. Blanchard, A. Kentner, S. Pustelny, A. Pines, and D. Budker, "Invited review article: Instrumentation for nuclear magnetic resonance in zero and ultralow magnetic field," *Review of Scientific Instruments*, vol. 88, no. 9, p. 091101, 2017.

[9] M. C. Tayler, J. Ward-Williams, and L. F. Gladden, "Ultralow-field nuclear magnetic resonance of liquids confined in ferromagnetic and paramagnetic materials," *Applied Physics Letters*, vol. 115, no. 7, p. 072409, 2019.

[10] P. Nikolaou, B. M. Goodson, and E. Y. Chekmenev, "NMR hyperpolarization techniques for biomedicine," *Chemistry (Weinheim an der Bergstrasse, Germany)*, vol. 21, no. 8, p. 3156, 2015.

[11] K. V. Kovtunov, E. V. Pokochueva, O. G. Salnikov, S. F. Cousin, D. Kurzbach, B. Vuichoud, S. Jannin, E. Y. Chekmenev, B. M. Goodson, D. A. Barskiy, *et al.*, "Hyperpolarized NMR spectroscopy: d-DNP, PHIP, and SABRE techniques," *Chemistry–An Asian Journal*, vol. 13, no. 15, pp. 1857–1871, 2018.

[12] O. Semenova, P. M. Richardson, A. J. Parrott, A. Nordon, M. E. Halse, and S. B. Duckett, "Reaction monitoring using sabre-hyperpolarized benchtop (1 T) NMR

spectroscopy," *Analytical chemistry*, vol. 91, no. 10, pp. 6695–6701, 2019.

[13] T. Theis, P. Ganssle, G. Kervern, S. Knappe, J. Kitching, M. Ledbetter, D. Budker, and A. Pines, "Parahydrogen-enhanced zero-field nuclear magnetic resonance," *Nature Physics*, vol. 7, no. 7, pp. 571–575, 2011.

[14] R. W. Adams, J. A. Aguilar, K. D. Atkinson, M. J. Cowley, P. I. Elliott, S. B. Duckett, G. G. Green, I. G. Khazal, J. López-Serrano, and D. C. Williamson, "Reversible interactions with para-hydrogen enhance NMR sensitivity by polarization transfer," *Science*, vol. 323, no. 5922, pp. 1708–1711, 2009.

[15] V. Yashchuk, J. Granwehr, D. Kimball, S. Rochester, A. Trabesinger, J. Urban, D. Budker, and A. Pines, "Hyperpolarized xenon nuclear spins detected by optical atomic magnetometry," *Physical review letters*, vol. 93, no. 16, p. 160801, 2004.

[16] R. Jiménez-Martínez, D. J. Kennedy, M. Rosenbluh, E. A. Donley, S. Knappe, S. J. Seltzer, H. L. Ring, V. S. Bajaj, and J. Kitching, "Optical hyperpolarization and NMR detection of 129 Xe on a microfluidic chip," *Nature communications*, vol. 5, no. 1, pp. 1–6, 2014.

[17] D. J. Kennedy, S. J. Seltzer, R. Jiménez-Martínez, H. L. Ring, N. S. Malecek, S. Knappe, E. A. Donley, J. Kitching, V. S. Bajaj, and A. Pines, "An optimized microfabricated platform for the optical generation and detection of hyperpolarized 129 Xe," *Scientific reports*, vol. 7, no. 1, pp. 1–10, 2017.

[18] M. P. Augustine, A. Wong-Foy, J. L. Yarger, M. Tomaselli, A. Pines, D. M. TonThat, and J. Clarke, "Low field magnetic resonance images of polarized noble gases obtained with a dc superconducting quantum interference device," *Applied physics letters*, vol. 72, no. 15, pp. 1908–1910, 1998.

[19] J. H. Ardenkjær-Larsen, B. Fridlund, A. Gram, G. Hansson, L. Hansson, M. H. Lerche, R. Servin, M. Thaning, and K. Golman, "Increase in signal-to-noise ratio of >10,000 times in liquid-state NMR," *Proceedings of the National Academy of Sciences*, vol. 100, no. 18, pp. 10158–10163, 2003.

[20] S. Jannin, J.-N. Dumez, P. Giraudeau, and D. Kurzbach, "Application and methodology of dissolution dynamic nuclear polarization in physical, chemical and biological contexts," *Journal of Magnetic Resonance*, vol. 305, pp. 41–50, 2019.

[21] B. Plainchont, P. Berruyer, J.-N. Dumez, S. Jannin, and P. Giraudeau, "Dynamic nuclear polarization opens new perspectives for nmr spectroscopy in analytical chemistry," 2018.

[22] S. J. Elliott, Q. Stern, M. Ceillier, T. El Daraï, S. F. Cousin, O. Cala, and S. Jannin, "Practical dissolution dynamic nuclear polarization," *Progress in Nuclear Magnetic Resonance Spectroscopy*, 2021.

[23] D. A. Barskiy, M. C. Tayler, I. Marco-Rius, J. Kurhanewicz, D. B. Vigneron, S. Cikrikci, A. Aydogdu, M. Reh, A. N. Pravdivtsev, J.-B. Hövener, *et al.*, "Zero-field nuclear magnetic resonance of chemically exchanging systems," *Nature communications*, vol. 10, no. 1, pp. 1–9, 2019.

[24] H.-Y. Chen and C. Hilty, "Implementation and characterization of flow injection in dissolution DNP-NMR," *Chemphyschem: a European journal of chemical physics and physical chemistry*, vol. 16, no. 12, p. 2646, 2015.

[25] T. El Daraï, S. F. Cousin, Q. Stern, M. Ceillier, J. Kempf, D. Eshchenko, R. Melzi, M. Schnell, L. Gremillard, A. Bornet, *et al.*, "Porous functionalized polymers enable generating and transporting hyperpolarized mixtures of metabolites," *Nature Communications*, vol. 12, no. 1, pp. 1–9, 2021.

[26] W. Köckenberger, "Dissolution dynamic nuclear polarization," *eMagRes*, pp. 161–170, 2007.

[27] P. Miéville, P. Ahuja, R. Sarkar, S. Jannin, P. R. Vasos, S. Gerber-Lemaire, M. Mishkovsky, A. Comment, R. Gruetter, O. Ouari, *et al.*, "Scavenging free radicals to preserve enhancement and extend relaxation times in NMR using dynamic nuclear polarization," *Angewandte Chemie International Edition*, vol. 49, no. 35, pp. 6182–6185, 2010.

[28] A. Bornet, J. Milani, B. Vuichoud, A. J. P. Linde, G. Bodenhausen, and S. Jannin, "Microwave frequency modulation to enhance dissolution dynamic nuclear polarization," *Chemical Physics Letters*, vol. 602, pp. 63–67, 2014.

[29] A. Bornet, R. Melzi, A. J. Perez Linde, P. Hautle, B. van den Brandt, S. Jannin, and G. Bodenhausen, "Boosting dissolution dynamic nuclear polarization by cross polarization," *The journal of physical chemistry letters*, vol. 4, no. 1, pp. 111–114, 2013.

[30] A. Bornet, A. Pinon, A. Jhajharia, M. Baudin, X. Ji, L. Emsley, G. Bodenhausen, J. H. Ardenkjaer-Larsen, and S. Jannin, "Microwave-gated dynamic nuclear polarization," *Physical Chemistry Chemical Physics*, vol. 18, no. 44, pp. 30530–30535, 2016.

[31] S. Jannin, A. Bornet, R. Melzi, and G. Bodenhausen, "High field dynamic nuclear polarization at 6.7 T: Carbon-13 polarization above 70% within 20 min," *Chemical Physics Letters*, vol. 549, pp. 99–102, 2012.

[32] A. Bornet, R. Melzi, S. Jannin, and G. Bodenhausen, "Cross polarization for dissolution dynamic nuclear polarization experiments at readily accessible temperatures 1.2<T<4.2 K," *Applied Magnetic Resonance*, vol. 43, no. 1, pp. 107–117, 2012.

[33] M. Jiang, R. P. Frutos, T. Wu, J. W. Blanchard, X. Peng, and D. Budker, "Magnetic gradiometer for the detection of zero-to ultralow-field nuclear magnetic resonance," *Physical Review Applied*, vol. 11, no. 2, p. 024005, 2019.

[34] D. Budker and M. Romalis, "Optical magnetometry," *Nature physics*, vol. 3, no. 4, pp. 227–234, 2007.

[35] H. J. Bernstein, J. A. Pople, and W. Schneider, "The analysis of nuclear magnetic resonance spectra: I. systems of two and three nuclei," *Canadian Journal of Chemistry*, vol. 35, no. 1, pp. 67–83, 1957.

[36] M. Emondts, M. P. Ledbetter, S. Pustelny, T. Theis, B. Patton, J. W. Blanchard, M. C. Butler, D. Budker, and A. Pines, "Long-lived heteronuclear spin-singlet states in liquids at a zero magnetic field," *Physical review letters*, vol. 112, no. 7, p. 077601, 2014.

[37] M. Ledbetter, C. Crawford, A. Pines, D. Wemmer, S. Knappe, J. Kitching, and D. Budker, "Optical detection of NMR J-spectra at zero magnetic field," *Journal of magnetic resonance*, vol. 199, no. 1, pp. 25–29, 2009.

[38] A. C. Pinon, A. Capozzi, and J. H. Ardenkjær-Larsen, "Hyperpolarization via dissolution dynamic nuclear polarization: new technological and methodological advances," *Magnetic Resonance Materials in Physics, Biology and Medicine*, pp. 1–19, 2020.

[39] P. Miéville, S. Jannin, and G. Bodenhausen, "Relaxometry of insensitive nuclei: optimizing dissolution dynamic nuclear polarization," *Journal of Magnetic Resonance*, vol. 210, no. 1, pp. 137–140, 2011.
[40] S. Bodenstedt, M. W. Mitchell, and M. C. Tayler, "Fast-field-cycling ultralow-field nuclear magnetic relaxation dispersion," *Nature Communications*, vol. 12, no. 1, pp. 1–8, 2021.
[41] I. V. Zhukov, A. S. Kiryutin, A. V. Yurkovskaya, Y. A. Grishin, H.-M. Vieth, and K. L. Ivanov, "Field-cycling NMR experiments in an ultra-wide magnetic field range: relaxation and coherent polarization transfer," *Physical Chemistry Chemical Physics*, vol. 20, no. 18, pp. 12396–12405, 2018.
[42] J. Zhu, E. Ye, V. Terskikh, and G. Wu, "Experimental verification of the theory of nuclear quadrupole relaxation in liquids over the entire range of molecular tumbling motion," *The Journal of Physical Chemistry Letters*, vol. 2, no. 9, pp. 1020–1023, 2011.
[43] M. C. Tayler and L. F. Gladden, "Scalar relaxation of NMR transitions at ultralow magnetic field," *Journal of Magnetic Resonance*, vol. 298, pp. 101–106, 2019.
[44] Y. Pocker, J. E. Meany, B. J. Nist, and C. Zadorojny, "Reversible hydration of pyruvic acid. I. equilibrium studies," *The Journal of Physical Chemistry*, vol. 73, no. 9, pp. 2879–2882, 1969.
[45] J. Eills, R. Picazo-Frutos, O. Bondar, E. Cavallari, C. Carrera, S. J. Barker, M. Utz, S. Aime, F. Reineri, D. Budker, *et al.*, "Metabolic reactions studied by zero-and low-field nuclear magnetic resonance," *arXiv preprint arXiv:2205.12380*, 2022.
[46] S. Alcicek, P. Put, D. Barskiy, V. Kontul, and S. Pustelny, "Zero-field nmr of urea: Spin-topology engineering by chemical exchange," *The journal of physical chemistry letters*, vol. 12, no. 43, pp. 10671–10676, 2021.
[47] P. Put, S. Pustelny, D. Budker, E. Druga, T. F. Sjolander, A. Pines, and D. A. Barskiy, "Zero-to ultralow-field nmr spectroscopy of small biomolecules," *Analytical Chemistry*, vol. 93, no. 6, pp. 3226–3232, 2021.
[48] J. W. Blanchard, T. Wu, J. Eills, Y. Hu, and D. Budker, "Zero-to ultralow-field nuclear magnetic resonance J-spectroscopy with commercial atomic magnetometers," *Journal of Magnetic Resonance*, vol. 314, p. 106723, 2020.
[49] M. Cavaillès, A. Bornet, X. Jaurand, B. Vuichoud, D. Baudouin, M. Baudin, L. Veyre, G. Bodenhausen, J.-N. Dumez, S. Jannin, *et al.*, "Tailored microstructured hyperpolarizing matrices for optimal magnetic resonance imaging," *Angewandte Chemie*, vol. 130, no. 25, pp. 7575–7579, 2018.
[50] D. Gajan, A. Bornet, B. Vuichoud, J. Milani, R. Melzi, H. A. Van Kalkeren, L. Veyre, C. Thieuleux, M. P. Conley, W. R. Grüning, *et al.*, "Hybrid polarizing solids for pure hyperpolarized liquids through dissolution dynamic nuclear polarization," *Proceedings of the National Academy of Sciences*, vol. 111, no. 41, pp. 14693–14697, 2014.
[51] D. Baudouin, H. A. Van Kalkeren, A. Bornet, B. Vuichoud, L. Veyre, M. Cavaillès, M. Schwarzwälder, W.-C. Liao, D. Gajan, G. Bodenhausen, *et al.*, "Cubic three-dimensional hybrid silica solids for nuclear hyperpolarization," *Chemical science*, vol. 7, no. 11, pp. 6846–6850, 2016.
[52] S. Bowen and C. Hilty, "Rapid sample injection for hyperpolarized NMR spectroscopy," *Physical Chemistry Chemical Physics*, vol. 12, no. 22, pp. 5766–5770, 2010.
[53] M. Ceillier, O. Cala, T. E. Daraï, S. F. Cousin, Q. Stern, S. Guibert, S. J. Elliott, A. Bornet, B. Vuichoud, J. Milani, C. Pages, D. Eshchenko, J. G. Kempf, C. Jose, S. A. Lambert, and S. Jannin, "An automated system for fast transfer and injection of hyperpolarized solutions," *Journal of Magnetic Resonance Open*, p. 100017, 2021.
[54] K. Kouřil, H. Kouřilová, S. Bartram, M. H. Levitt, and B. Meier, "Scalable dissolution-dynamic nuclear polarization with rapid transfer of a polarized solid," *Nature communications*, vol. 10, no. 1, pp. 1–6, 2019.
[55] M. Leutzsch, A. J. Sederman, L. F. Gladden, and M. D. Mantle, "In situ reaction monitoring in heterogeneous catalysts by a benchtop NMR spectrometer," *Magnetic resonance imaging*, vol. 56, pp. 138–143, 2019.
[56] M. C. Tayler, J. Ward-Williams, and L. F. Gladden, "NMR relaxation in porous materials at zero and ultralow magnetic fields," *Journal of Magnetic Resonance*, vol. 297, pp. 1–8, 2018.
[57] P. A. Boeg, J. Ø. Duus, J. H. Ardenkjær-Larsen, M. Karlsson, and S. Mossin, "Real-time detection of intermediates in rhodium-catalyzed hydrogenation of alkynes and alkenes by dissolution dnp," *The Journal of Physical Chemistry C*, vol. 123, no. 15, pp. 9949–9956, 2019.
[58] M. C. Butler, G. Kervern, T. Theis, M. P. Ledbetter, P. J. Ganssle, J. W. Blanchard, D. Budker, and A. Pines, "Parahydrogen-induced polarization at zero magnetic field," *The Journal of Chemical Physics*, vol. 138, no. 23, p. 234201, 2013.

Appendix A: Observable transition for a two-spin system at zero field

We show the relation between the signal intensity observed at zero field for a pair of J-coupled spin-1/2 I and S and their respective polarization P_I and P_S.

Whether the pair of spins was hyperpolarized by dDNP or thermally prepolarized in a permanent magnet, the initial density matrix expressed in the Zeeman basis can be written as

$$\hat{\rho}_0 = p_{\alpha\alpha}\hat{\rho}_{\alpha\alpha} + p_{\alpha\beta}\hat{\rho}_{\alpha\beta} + p_{\beta\alpha}\hat{\rho}_{\beta\alpha} + p_{\beta\beta}\hat{\rho}_{\beta\beta}, \tag{A1}$$

where $p_{\alpha\alpha}$, $p_{\alpha\beta}$, $p_{\beta\alpha}$ and $p_{\beta\beta}$ are the populations of the Zeeman states related to the nuclear polarization P_I and P_S by

$$
\begin{aligned}
p_{\alpha\alpha} &= \frac{1 + P_I + P_S + P_I P_S}{4} \\
p_{\alpha\beta} &= \frac{1 + P_I - P_S - P_I P_S}{4} \\
p_{\beta\alpha} &= \frac{1 - P_I + P_S - P_I P_S}{4} \\
p_{\beta\beta} &= \frac{1 - P_I - P_S + P_I P_S}{4} \,.
\end{aligned}
\tag{A2}
$$

A sudden transition from high field to zero field projects the Zeeman states onto the zero-field states, which are given by the singlet-triplet basis:

$$
\begin{aligned}
|T_+\rangle &= |\alpha\alpha\rangle \\
|T_0\rangle &= \left(|\alpha\beta\rangle + |\beta\alpha\rangle\right)/\sqrt{2} \\
|S_0\rangle &= \left(|\alpha\beta\rangle - |\beta\alpha\rangle\right)/\sqrt{2} \\
|T_-\rangle &= |\beta\beta\rangle \,.
\end{aligned}
\tag{A3}
$$

Conversely, the Zeeman states can be expressed in terms of the singlet and triplet states

$$
\begin{aligned}
|\alpha\alpha\rangle &= |T_+\rangle \\
|\alpha\beta\rangle &= \left(|T_0\rangle + |S_0\rangle\right)/\sqrt{2} \\
|\beta\alpha\rangle &= \left(|T_0\rangle - |S_0\rangle\right)/\sqrt{2} \\
|\beta\beta\rangle &= |T_-\rangle \,.
\end{aligned}
\tag{A4}
$$

Similarly to reference [58], we define a set of zero- and double-quantum operators as

$$
\begin{aligned}
\hat{Z}_x &= \hat{I}_x\hat{S}_x + \hat{I}_y\hat{S}_y \\
\hat{Z}_y &= \hat{I}_x\hat{S}_y - \hat{I}_y\hat{S}_x \\
\hat{Z}_z &= \frac{1}{2}\left(\hat{I}_z - \hat{S}_z\right) \\
\hat{D}_z &= \frac{1}{2}\left(\hat{I}_z + \hat{S}_z\right)
\end{aligned}
\tag{A5}
$$

that obey the cycling commutation relation

$$
\begin{aligned}
[\hat{Z}_x, \hat{Z}_z] &= i\hat{Z}_y \\
[\hat{Z}_y, \hat{Z}_x] &= i\hat{Z}_z \\
[\hat{Z}_z, \hat{Z}_y] &= i\hat{Z}_x \,,
\end{aligned}
\tag{A6}
$$

meaning that $\hat{Z}_x$ converts $\hat{Z}_z$ into $\hat{Z}_y$ and $\hat{Z}_y$ into $-\hat{Z}_z$. We note that the $\hat{Z}_z$ and $\hat{D}_z$ operators can be written as

$$
\begin{aligned}
\hat{Z}_z &= \frac{1}{2}\left(|T_0\rangle\langle S_0| + |S_0\rangle\langle T_0|\right) \\
\hat{D}_z &= \frac{1}{2}\left(\hat{T}_+ + \hat{T}_-\right) .
\end{aligned}
\tag{A7}
$$

The elements of the initial density matrix written in the Zeeman basis in Eq. A1 can be written in terms of the zero-field operators as

$$
\begin{aligned}
\hat{\rho}_{\alpha\alpha} &= \hat{T}_+ \\
\hat{\rho}_{\alpha\beta} &= |\alpha\beta\rangle\langle\alpha\beta| = \frac{1}{2}\left(|T_0\rangle\langle T_0| + |S_0\rangle\langle S_0| + |T_0\rangle\langle S_0| + |S_0\rangle\langle T_0|\right) = \frac{1}{2}\left(\hat{T}_0 + \hat{S}_0 + 2\hat{Z}_z\right) \\
\hat{\rho}_{\beta\alpha} &= |\beta\alpha\rangle\langle\beta\alpha| = \frac{1}{2}\left(|T_0\rangle\langle T_0| + |S_0\rangle\langle S_0| - |T_0\rangle\langle S_0| - |S_0\rangle\langle T_0|\right) = \frac{1}{2}\left(\hat{T}_0 + \hat{S}_0 - 2\hat{Z}_z\right) \\
\hat{\rho}_{\beta\beta} &= \hat{T}_-,
\end{aligned}
\tag{A8}
$$

and so we can write the initial density matrix as

$$
\begin{aligned}
\hat{\rho}_0 &= p_{\alpha\alpha}\hat{T}_+ + p_{\alpha\beta}\frac{1}{2}\left(\hat{T}_0 + \hat{S}_0 + 2\hat{Z}_z\right) + p_{\beta\alpha}\frac{1}{2}\left(\hat{T}_0 + \hat{S}_0 - 2\hat{Z}_z\right) + p_{\beta\beta}\hat{T}_- \\
&= p_{\alpha\alpha}\hat{T}_+ + \frac{p_{\alpha\beta} + p_{\beta\alpha}}{2}\left(\hat{T}_0 + \hat{S}_0\right) + \left(p_{\alpha\beta} - p_{\beta\alpha}\right)\hat{Z}_z + p_{\beta\beta}\hat{T}_-,
\end{aligned}
\tag{A9}
$$

where we plug in the relation of Eq. A2 to get

$$
\hat{\rho}_0 = \frac{1 + P_I + P_S + P_I P_S}{4}\hat{T}_+ + \frac{1 - P_I P_S}{4}\left(\hat{T}_0 + \hat{S}_0\right) + \frac{P_I - P_S}{2}\hat{Z}_z + \frac{1 - P_I - P_S + P_I P_S}{4}\hat{T}_- \,. \tag{A10}
$$

The Hamiltonian at zero field only consists of the J-interaction

$$
\hat{H}_J = 2\pi J \hat{\boldsymbol{I}} \cdot \hat{\boldsymbol{S}} = 2\pi J\left(\hat{Z}_x + \hat{I}_z\hat{S}_z\right) \,. \tag{A11}
$$

Equations A3 and A5 allow the following re-expression of the operators:

$$
\begin{aligned}
\hat{T}_\pm &= \hat{1}/4 + \hat{I}_z\hat{S}_z \pm \hat{D}_z \\
\hat{T}_0 + \hat{S}_0 &= \hat{1}/2 - 2\hat{I}_z\hat{S}_z \,,
\end{aligned}
\tag{A12}
$$

and it can readily be shown that $[\hat{I}_z\hat{S}_z, \hat{H}_J] = [\hat{D}_z, \hat{H}_J] = 0$. Because of this, we can rewrite the initial density matrix and the Hamiltonian (Eq, A10 and A11, respectively) keeping only the non-commuting terms and so we get

$$
\hat{\rho}_0 = \frac{P_I - P_S}{2}\hat{Z}_z \tag{A13}
$$

and

$$
\hat{H}_J = 2\pi J \hat{Z}_x. \tag{A14}
$$

The cyclic commutation relation of Eq. A6 give the time evolution of the density matrix at zero field [2, 58]

$$
\hat{\rho}(t) = \frac{P_I - P_S}{2}\left[\cos\left(2\pi J t\right)\hat{Z}_z + \sin\left(2\pi J t\right)\hat{Z}_x\right] \,, \tag{A15}
$$

which gives rise to observable magnetization oscillating at frequency $2\pi J$

$$
\begin{aligned}
M_z(t) &= \mathrm{Tr}\left[\left(\gamma_I\hat{I}_z + \gamma_S\hat{S}_z\right)\hat{\rho}(t)\right] \\
&= \frac{P_I - P_S}{2}\left[\gamma_I\mathrm{Tr}\left(\hat{I}_z\hat{Z}_z\right) + \gamma_S\mathrm{Tr}\left(\hat{S}_z\hat{Z}_z\right)\right]\cos\left(2\pi J t\right) \\
&= \frac{P_I - P_S}{4}\left(\gamma_I - \gamma_S\right)\cos\left(2\pi J t\right).
\end{aligned}
\tag{A16}
$$

This shows that there is one line in the spectrum (at the J-coupling frequency) and that the signal is proportional to the difference in polarization of the two spins.